Spectroscopic Studies of Polymer Interdiffusion during Film Formation

Elisa M. Boczar,* B. Camille Dionne, Zhenwen Fu, Andrea B. Kirk, Patricia M. Lesko, and Anne D. Koller

Rohm and Haas Company, 727 Norristown Road, Spring House, Pennsylvania 19477

Received April 12, 1993; Revised Manuscript Received July 19, 1993®

ABSTRACT: Polymer interdiffusion between latex particles during film formation is studied using the fluorescence technique of nonradiative energy transfer (NET). Model emulsion polymers of poly(butyl methacrylate) and poly(amyl methacrylate), labeled with the energy transfer pair of 1-naphthylethyl methacrylate or 9-anthryl methacrylate, are investigated. The effects of particle size, polymer glass transition temperature, and polymer compatibility on the rate and extent of interparticle diffusion are measured. In addition, the time dependence of transmission electron microscopy images during the final stage of film formation augments the conceptual picture of interdiffusion. A change in particle size is observed to enhance the intermixing rate in proportion to the particle surface area to volume ratio, while leaving the apparent diffusion coefficient unchanged. The dependence of the diffusion coefficient on temperature is adequately described by both the WLF and Arrhenius equations, albeit throughout a comparatively narrow temperature range, and the activation energies were found to be equivalent within experimental error for the two acrylates. The extent of polymer interdiffusion in a film formed from a blend of the two methacrylate compositions appears to be affected by the compatibility of the components.

I. Introduction

The evolution of polymeric coatings from solvent-based to aqueous emulsion technologies has required an understanding of processes unique to latex dispersions. One of these fundamental processes is the transformation of particles in a stable latex dispersion into a continuous polymer film. Obviously, film formation is a critical aspect of all latex applications that involve coating a surface or forming a sheet. In an idealized model, film formation has been conceptually separated into three transitions between four states,[1-3] as depicted in Figure 1. The first state corresponds to the "wet state" of the latex: solid polymer "hard spheres" dispersed in water, typically at 20-50% by weight. After evaporation of most of the water, state II is formed. State II is described as an ordered packing of emulsion particles with residual water in the interparticle voids. Above the glass transition temperature, further evaporation and other intermolecular interactions combine to produce particles in state III, which have compacted and deformed but still retain a distinct identity from particle to particle.

In the final stage of the film formation process, interdiffusion of polymer chains across the latex particle boundaries eventually blurs the distinctions between particles and results in state IV, a continuous homogeneous film. This evolution from state I to state IV is described for an ideal system. In real systems, the situation is more complex due to inhomogeneities and the presence of various formulation components, such as surfactant, pigment, etc.

Experimentally, study of the final stage of film formation has lagged behind that of the first two stages. In the past several years, two techniques, small-angle neutron scattering (SANS) and nonradiative energy transfer (NET), have been utilized to study the interdiffusion process directly. SANS can effectively follow the "growth" in particle size of deuterated latex particles as self-diffusion progresses. The first reports of work of this type came from Hahn and co-workers[4,5] in 1986 using butyl methacrylate (BMA) polymers. Linne et al.[6] used SANS to measure an actual interdiffusion depth and relate it to toughness measurements in polystyrene. More recently, the same group[7,8] published work on polystyrene films and reached the conclusion that the location of chain ends and the ratio of the chain radii of gyration to the particle size are two critical parameters for interdiffusion.

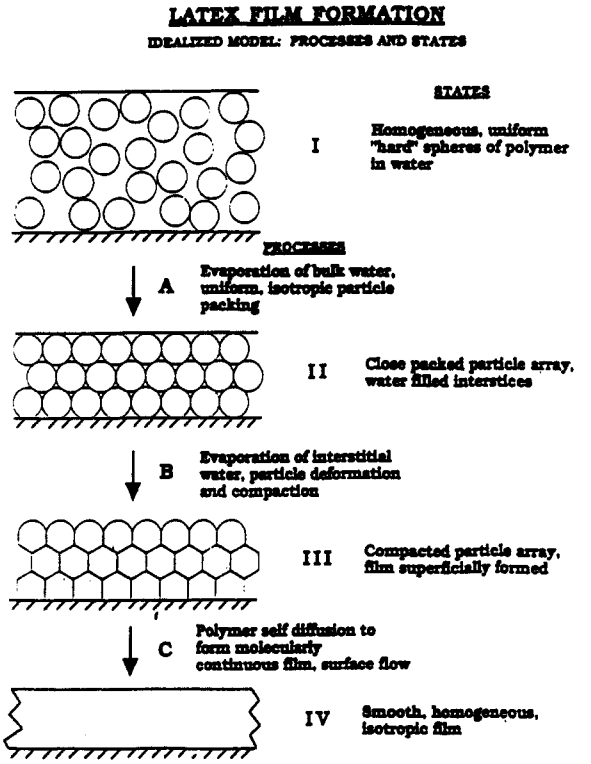

Figure 1. A schematic depicting the three stages of film formation (courtesy of P. R. Sperry, Rohm and Haas).

Energy transfer techniques may also be used to study interdiffusion directly during film formation, and such accounts have been published by Winnik and co-workers at the University of Toronto.[9,10] Following their work, we have employed this technique, monitoring fluorescence lifetime changes due to NET, to probe the interdiffusion process. The experiments detailed here were designed to

® Abstract published in *Advance ACS Abstracts*, September 15, 1993.

0024-9297/93/2226-5772$04.00/0

study the rate and extent of the polymer interdiffusion process in films and to explore how this is affected by parameters of latex design.

II. Theoretical Development and Data Analysis

Although energy transfer has been observed in polymer systems for quite some time,[11] it was Morawetz, in 1984, who demonstrated that energy transfer between chromophore-labeled polymer molecules could be used to detect the slow rates of self-diffusion in methyl methacrylate (MMA)/ethyl methacrylate (EMA) solution polymers.[12] Winnik has successfully applied this technique specifically to latex polymers and refined it to the extent that fractions of mixing and diffusion coefficients may be calculated with relative ease.

The basis of the technique is the phenomenon of dipole–dipole energy transfer, first described theoretically by Förster in 1948.[13] This NET from the donor to the acceptor can effectively reduce the normal donor emission lifetime. In addition to spectral overlap, there is a spatial requirement for efficient energy transfer, namely that the two participating chromophores be within a certain characteristic distance. This distance, the "Förster radius", R_0, is equal to the distance where the probability for quenching is equal to the probability for normal fluorescence. R_0 is equal to about 23 Å[14] for the naphthyl/anthryl pair, and energy transfer is measurable up to about twice R_0, or distances approaching 40 Å (4 nm).

The phenomenon of energy transfer may be exploited to follow interdiffusion in films in the following way. An emulsion is prepared in which half of the latex particles consist of polymer chains labeled with a suitable donor chromophore and the other half of the particles consist of polymer chains labeled with an appropriate acceptor chromophore. To retain most of the original, unlabeled polymer's physical properties, the concentration of the chromophore tags is kept low, about 1% by weight. As the emulsion is drawn down, water evaporates and film formation begins. During the latter stages of this process, interdiffusion occurs between tagged polymer molecules in adjacent latex particles. As interdiffusion proceeds, the fluorescence of an increasing number of naphthyl groups is quenched by anthryl groups that have diffused into neighboring particles. Thus, monitoring the naphthyl lifetime as a function of real time as a film forms enables us to probe the extent of mixing between latex particles.

The measured fluorescence time profile, $I(t)$, of a system undergoing energy transfer is described by the Förster equation.[15] This relationship governs the molecules in the "mixed" domain where interpenetration has already occurred. The "unmixed" domain is a region where no interdiffusion, and therefore no energy transfer, has taken place. In this spatial region the naphthyl emission can be approximately by a single exponential.[16] Combining equations and assuming a uniform distribution of tag molecules in an ideally packed particle array yields

$$I(t) = B_1 \exp((-t/\tau_0) - \beta(t/\tau_0)^{1/2}) + B_2 \exp(-t/\tau_0) \quad (1)$$

where τ_0 is the fluorescence lifetime of the donor chromophore in the absence of any quenching species, B_1 represents the number of molecules in the interpenetrated region, and B_2 represents the number in the unmixed region. The parameter β is defined as[17]

$$\beta = {}^4/_3\pi^{3/2}N\{A\}R_0^3 \quad (2)$$

where N is 6.023×10^{-20}, $\{A\}$ is the molar concentration of acceptor molecules, and R_0 is the critical transfer distance (in angstroms) for the donor/acceptor pair. R_0 depends on the spectral overlap between donor and acceptor, the refractive index of the medium, the acceptor oscillator strength, and the quantum yield and orientation of the donor chromophore.[17]

Other theoretical models have been proposed to analyze the donor decay profile that explicitly include a correlation function between donor and acceptor species. Using this type of scheme would, in turn, require adopting a specific diffusion model at this point and calculating the concentration of donor and acceptor species as a function of time. This type of analysis demands a much more complex treatment of the concentration profile in the film. We choose to make the simplifying assumptions that the mixed and unmixed domains are sharply divided and that the acceptor concentration is isotropic throughout the mixed area.[18]

Other assumptions include presuming that an equal number of donor and acceptor moieties are present initially and that the volumes occupied by donor and acceptor moieties are equal. It is also implied that the concentration of donor groups in the unmixed region is equal to twice the concentration in the mixed region. It is evident that this last assumption will be true at long times when the initial concentration of donors is effectively diluted by its migration into a space of twice its original volume. This leads to the complementary assumption that the concentration of acceptor groups remains constant throughout the experiment. The acceptor concentration has been calculated as a function of fraction of mixing to demonstrate the validity of this assumption.[18] It was found that it does indeed remain relatively constant but not quite at the predicted level.

Our assumptions regarding the concentration allow us to analyze the data in terms of a volume fraction of mixing, F_m, equal to

$$F_m = B_1/(B_1 + B_2) \quad (3)$$

F_m is a quantitative measure of the extent of interpenetration between latex particles. F_m should increase during the cure, with a value of 1 representing a totally mixed system.

In a fashion independent of the Förster treatment of the lifetime data, we have developed a model that will enable us to extract diffusion coefficients from the fraction of mixing data. The ability to calculate diffusion coefficients allows us to quantitatively compare diffusion rates between different polymer systems and to evaluate our experimental results with those from vastly different techniques. The numerical values of the coefficients themselves are less important and not the direct goal of our work.

We consider first a naphthyl-labeled latex particle with a radius R. As interdiffusion occurs in three dimensions between this particle and the 12 nearest neighbor particles surrounding it, the unperturbed region can be approximated by a sphere of radius r (at first equal to R). We appreciate that in the nascent film a dodecahedral geometry is more accurate than spherical, but this approximation is probably not severe. Furthermore, we must assume uniform packing of the coalesced particles, and indeed TEM results demonstrate that locally the packing is fairly regular. Figure 2 shows an illustration of our spherical model where anthryl moieties (A) have diffused a distance l into the original naphthyl-labeled particle (N) creating a shell of mixed naphthyl/anthryl labels surrounding a naphthyl-only core.

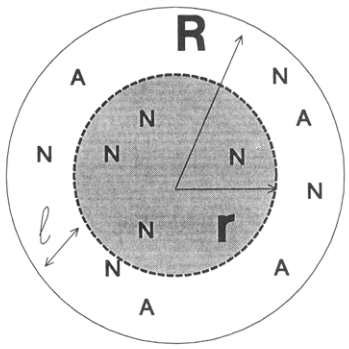

Figure 2. A diagram of the simple spherical diffusion model developed in this work. Anthryl- and naphthyl-tagged polymers are represented by "A" and "N", respectively. The original N-labeled particle has a radius R, while the A-labeled polymer has invaded the particle through a distance l.

We define the interdiffusion length, l, by

$$l = R - r \tag{4}$$

This distance represents the effective increase in the particle size due to diffusion outward from the core. According to Fick's law[19] for three-dimensional diffusion, the interdiffusion length is proportional to the square root of time through

$$l = (6Dt)^{1/2} \tag{5}$$

The proportionality constant is the diffusion coefficient, D. Rearrangement and substitution yield

$$r = R - (6Dt)^{1/2} \tag{6}$$

We also define the volume fraction of mixing, F_m, as

$$F_m(t) = ({}^4/_3\pi R^3 - {}^4/_3\pi r^3)/({}^4/_3\pi R^3) = 1 - r^3/R^3 \tag{7}$$

Substitution and expansion of the cubic term and rearrangement result in the following expression:

$$F_m(t) = a_0 + a_1 t^{1/2} + a_2 t + a_3 t^{3/2} \tag{8}$$

where

$$a_1 = 3(6D/R)^{1/2} \tag{9}$$

$$a_2 = -18D/R^2 \tag{10}$$

$$a_3 = (6D/R)^{3/2} \tag{11}$$

Since R, the particle radius, is known, we can fit our experimentally derived $F_m(t)$ data to this equation and obtain a value for D. The D we calculate is a mean translational diffusion coefficient and is an average D throughout the time scale of our measurement and also an average over the molecular weight distribution of the sample. We would expect that the lower molecular weight species would dominate the diffusion process at early times. An alternative procedure is to calculate a unique diffusion coefficient at each F_m point. This cumulative (rather than average) D changes over time throughout the course of the experiment. Again, this change is probably related to the change in the specific molecular weight component giving rise to the fluorescence signal at a given time.

From the literature[18,20] it appears that at short times (t < the chain reptation time T_r) the diffusion does not obey Fick's law in that mass transfer is not proportional to $t^{1/2}$. This may be traced, at least in part, to the relaxation of polymer chains at the particle surface. These chains have been deformed from their equilibrium configurations by their confinement in a particle whose diameter is less than R_g. After some initial period, the diffusion appears to be able to be fit to a Fickian form, but the physical meaning of this result remains unclear. Also, the presence of water-soluble additives, perhaps located in interstitial voids, may also affect the rate.

Our diffusion model does not explicitly consider the concentration of either donor or quencher species. In a more complex analysis used by Winnik et al., a spherical diffusion model is also employed.[9,10] In their treatment, an expression is used that describes the concentration as a function of the radial diffusion length and time. In our case, concentration is approximated by essentially a step function between mixed and unmixed regions. The concentration of the unmixed region is the initial naphthyl concentration, C_0, and the concentration in the mixed region is the final concentration, $C_0/2$.

Table I

reagent (g/100 g of latex)	100-nm latex	300-nm latex
monomer[a]	42.5	34.0
SDBS[b]	0.17	0.067
ammonium persulfate	0.19	0.15
100-nm seed polymers[c]	0	1.18

[a] Total weight of all monomers including the fluorophore tags. [b] Sodium dodecyl benzenesulfonate. [c] Dry weight of polymer solids.

III. Experimental Section

The 1-naphthylethyl methacrylate (NEMA) monomer was prepared by reaction of methacryloyl chloride and 1-naphthaleneethanol in base.[21] Purification of the NEMA monomer was accomplished by column chromatography and checked by thin-layer chromatography, IR, and NMR. The 9-anthryl methacrylate (AnMA) monomer was synthesized by reacting methacryloyl chloride and the enol forms of anthrone in base.[10] The AnMA was purified by recrystallization from ethanol and characterized by IR and NMR.

All polymers were prepared by a 3-h, semicontinuous emulsion polymerization, with persulfate initiation at 85 °C. The polymerization surfactant was sodium dodecyl benzenesulfonate, and the 300-nm BMA latex was seeded with a 100-nm particle. The amounts of the reagents used are summarized in Table I.

The level of fluorescent labeling is nominally 1.0 wt % AnMA and 0.91 wt % NEMA, equivalent molar amounts. One weight percent corresponds to an average of roughly 15 chromophores per chain. This type of monomer-starved polymerization was chosen to promote a random distribution of chromophores along each polymer chain. GPC results demonstrate that there are no asymmetries between the traces recorded using a refractive index and an ultraviolet absorption detector, indicating a uniform incorporation of the labels.

There is evidence for an impurity present in the naphthyl monomer sample. That is, there is a peak in the GPC trace with about 5% the area of the NEMA monomer peak. The molecular weight of the impurity is consistent with a NEMA dimer bonded through an ether linkage. The low level of this impurity does not significantly affect the results, and any effect would be constant throughout all of the experiments since all involved samples have a component polymerized with this monomer.

The physical characterization of the samples is summarized in Table II. Latex particle sizes were determined by photon correlation spectroscopy, using a Brookhaven BI-90 instrument. Molecular weights were determined by GPC on freeze-dried polymer subsequently dissolved in THF and calibrated against PMMA standards. Minimum film formation temperatures (MFFT's) were measured on a Sheen Instruments SS-3000 MFT bar. Glass transition temperatures (T_g's) of freeze-dried emulsions were measured on a DuPont 912 DSC and recorded as reheat half-height midpoint values. Residual BMA monomer was found to be <100 ppm. Data are also provided on the analogous unlabeled materials. On the whole, the data indicate that the chromophore tags do not significantly perturb these properties of the polymers.

Five-mil films were drawn down on glass slides. A convection oven purged with nitrogen gas was equilibrated at the target

Table II. Physical Properties of Polymers Used in Energy Transfer Experiments: *p*-Butyl Methacrylate and Amyl Methacrylate Polymers

composition	particle size (nm)	mol wt (×1000) M_w	M_n	M_w/M_n	% solids	MFFT (°C)	T_g (°C)
100 BMA	113	365	162	2.25	42	39	33
99 BMA/1 NEMA	108	384	145	2.64	42	40	31
99 BMA/1 AnMA	105	372	160	2.33	41	40	33
99 BMA/0.5 NEMA/ 0.5 AnMA	109	330	137	2.4	41	40	33
100 BMA	281	380	155	2.45	34	35	31
99 BMA/1 NEMA	297	333	139	2.40	34	34	32
99 BMA/1 AnMA	288	311	123	2.53	34	41	35
99 AmMA/1 NEMA	101	180	52	3.46	38	18	17
99 AmMA/1 AnMA	105	193	59	3.27	37	18	16

temperature before the introduction of the samples and maintained to within ±2 °C. After a film was heated for a specific time interval, it was removed from the oven and cooled to room temperature, and its fluorescence lifetime was measured. Since the T_g's of these polymers are near room temperature or above, no interdiffusion occurs during the measurement process. After the lifetime measurement, which typically took 20 min, the films were placed back into the oven and the curing was recommenced. A fresh sample was prepared for each temperature series.

The fluorescence decay time of a naphthyl-only film was measured to be approximately 65 ns. Curing at 100 °C for 48 h induces no reduction in lifetime. This indicates that no impurity in the naphthyl emulsion is causing quenching. After 7 months at room temperature, the lifetime for this film had remained constant. Therefore, for BMA we use 65 ns as the τ_0 for all fits to the Förster equation, with the exception of work involving the polymer blends. For those fits, a τ_0 that is basically an average of the τ_0 of the individual blend components was used for the mixed region, while the unmixed regions were represented by the τ_0 of the pure component.

Following introduction of the quenching species (50/50 blend of anthryl- and naphthyl-tagged particles), the lifetime drops from 66 to about 63 ns in the latex. A possible explanation for this decrease would be quenching by unbound anthryl tag molecules. However, GPC results have shown that the AnMA is completely incorporated into the polymer phase (within the detection limit of 100 ppm). Alternatively, we consider surface quenching by particles that are within twice R_0. A rough calculation indicates that the average distance between two 300-nm emulsion particle surfaces at the solids level of our samples is about 600 Å, over an order of magnitude greater than the maximum distance for energy transfer. However, this is an average and a wide distribution of interparticle distances is expected. Conceivably, there could be some surface contact interaction. In any event, the effect is small and should be constant throughout our experiments.

We define an "initial condition" for all subsequent curing experiments for the BMA polymers of 42 °C for 20 min. This aging represents the approximate disappearance of opacity in the films and thus corresponds more to a visual MFFT rather than to a DSC T_g. In the 50 naphthyl/50 anthryl (100 nm) film, the initial condition curing results in a lifetime of 61.7 ns. The slight drop of the lifetime from that of the latex (~63 ns) to the film (~62 ns) could be evidence of particle coalescence during the first two stages of film formation.[22] Initially, there will be some interparticle energy transfer without any interdiffusion between particles, due solely to surface contact of the particles. However, it should be noted that the lifetime of the initial condition film is stable at room temperature for over 7 months, indicating that the rate of interdiffusion at this temperature is beyond our detection limits.

To generate a model for extensive mixing, a film was cast from equal amounts of naphthyl- and anthryl-tagged BMA polymers dissolved in THF. In addition, a "colabeled" sample was polymerized by the simultaneous introduction of both fluorescent tags into the monomer mix. The solvent-cast film gives a lifetime of 49.6 ns after the initial cure. However, the colabeled sample yields the lowest decay time of all the films, 42.5 ns, which remained constant over 7 months at room temperature. The methodology used for developing controls was similar for experiments on the 300-nm particle size BMA and AmMA latices.

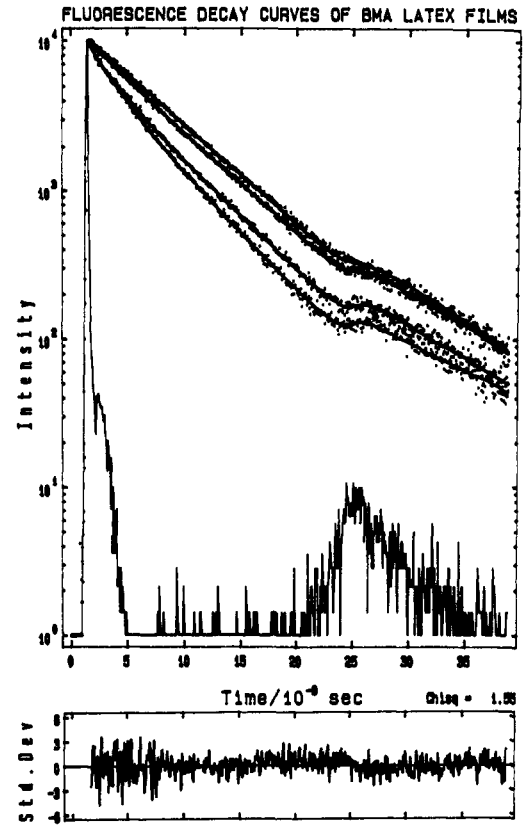

Figure 3. Fluorescence decay curves of (top to bottom) a naphthyl-only BMA film (a) and a 50/50 naphthyl/anthryl-tagged BMA film cured for 0 (b), 5 (c), and 120 (d) min at 100 °C. The data are fit to the Förster equation as described in the text. The feature at long times is part of the flashlamp profile, which is deconvoluted from the decays prior to analysis. The residual plot at the bottom of the figure corresponds to curve a.

An Edinburgh Model 199 lifetime spectrometer was used throughout for recording the decay curves. A pulsed hydrogen flashlamp selectively excites the naphthalene chromophore at 280 nm. The excitation is focused onto the film, and the emission is monitored at a 90° angle to the excitation. The fluorescence is observed at 340 nm through a Corning 0-53 filter. A Philips XP2020Q photomultiplier tube operating in a time-correlated single-photon-counting mode is used as a detector, and the raw data are stored on disk. The data are first deconvoluted from an instrument response function that was approximately 2-4-ns fwhm. Typically, data are collected from 20 to 360 ns after the excitation pulse. We calculate a precision of about ±0.3 ns for fluorescence lifetimes measured on our apparatus.

Transmission electron microscopy (TEM) was also used to characterize the interdiffusion in BMA latex films cast from 20% anthryl-labeled BMA mixed with 80% unlabeled BMA. Cross-sectioned specimens were obtained via microtomy. Typical section thicknesses were on the order of 100 nm. The sections were supported on Formvar-coated copper grids and exposed to the vapors of RuO_4 to enhance image contrast.[23] The anthryl-labeled BMA latex produced greater contrast with the staining than the naphthyl-labeled counterpart and is thus shown here. Similar results were obtained regardless of which tag was examined. Micrographs were acquired using a JEOL 1200 CX TEM operating at 60 keV.

IV. Results on Interdiffusion in BMA Films

A. Effect of Cure Time and Temperature. Initial results on the effect of cure time and temperature were accomplished using the 100-nm particle size BMA latex. Figure 3 shows a set of raw decay curves obtained for a

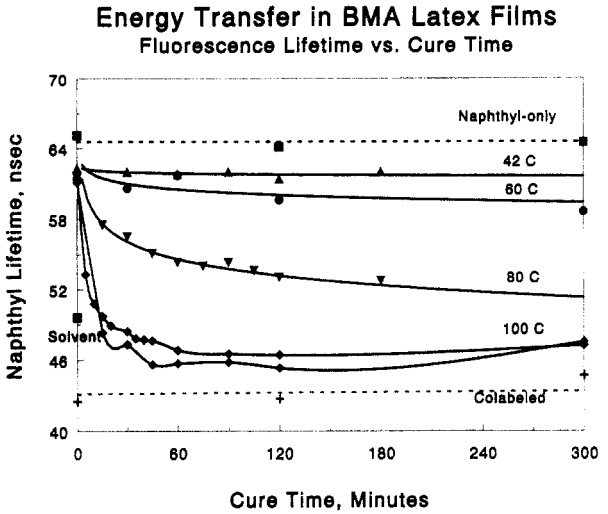

Figure 4. Data for BMA films tagged 50/50 with the naphthyl/anthryl energy transfer pair. The figure shows plots of the raw fluorescence data in the form of the naphthyl lifetime as a function of film cure time at various temperatures. Lines through the data are for visual clarity only. In addition, data are provided from control films which serve as models for both ends of the mixing scale and also remain constant with time.

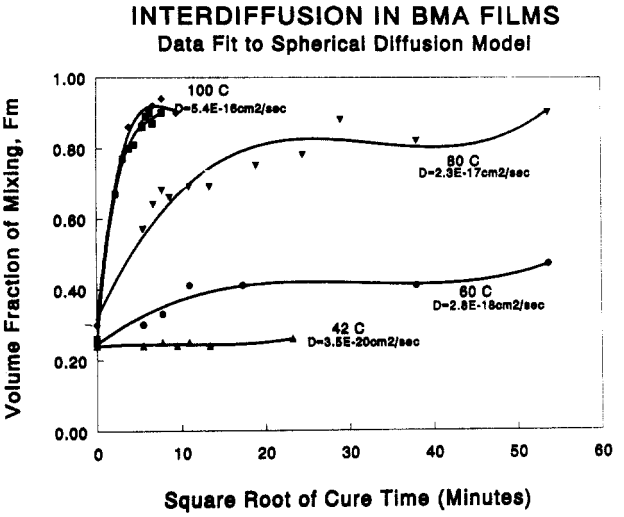

Figure 5. Using the raw data from Figure 3, individual decay curves are first fit to the Förster equation to generate a volume fraction of mixing, F_m. At each temperature, the data are then fit to the spherical diffusion model to produce the third-order polynomial curves shown here, yielding an average diffusion coefficient.

naphthyl-only BMA film (a) and a 50/50 naphthyl/anthryl BMA film after 0, 5, and 120 min at 100 °C (b, c, and d). The lifetime decreases as interdiffusion progresses and is evidenced by the increased curvature of the decays, particularly at early times. When fit to the Förster equation, χ^2 values obtained are typically 1.6. The Förster equation assumes a single-exponential decay for naphthalene in the absence of quencher. When the naphthyl-only data are fit, a double-exponential analysis yield a slightly lower χ^2 (about 1.5) than does a single-exponential fit ($\chi^2 \cong 1.7$). However, we proceed with the Förster fits since this deviation is not large.

Figure 4 depicts a series of plots illustrating the decrease in naphthyl lifetime in BMA films as a function of cure time at four different cure temperatures. Each point represents an experimentally determined biexponential lifetime, while the lines connecting the points are merely a visual aid. These data are derived from films cured for up to 5 h. At 42 °C the data show no change in naphthyl lifetime with cure time, confirming the lack of significant intermixing during the slight heating required to prepare the samples. The initial lifetimes (at time zero) for the samples in these series are all within 61.7 ± 0.5 ns.

The temperature dependence of the interdiffusion rate is quite dramatic. There is a slow but measurable change in the lifetime of the film cured at 60 °C during the first 5 h. By 100 °C, the lifetime reaches a more or less constant value within the first hour of cure. The data at 100 °C include a duplicate run at the same temperature, giving an idea of the overall error involved in the method. Also included in Figure 4 are the results from the control films that effectively bracket the data. After 2 days (not shown), the data at 80 and 100 °C appear to be converging to a common final value, while the lifetime of the film cured at 60 °C may or may not have plateaued.

The fluorescence decay curves represented by each data point of Figure 4 were then fit individually to the Förster equation as described previously. The fraction of mixing values, F_m, versus time are plotted in Figure 5. We note first that the F_m's at time zero (the y intercepts of the curves) are nonzero. This implies some interaction between naphthyl and anthryl groups in the nascent film at our definition of time zero. a nonzero intercept is expected since chromophores on the surfaces of adjacent latex particles can experience energy transfer. We calculate an estimated 0.13 F_m for 100-nm particles based on contact through a shell with a thickness equal to the critical Förster distance (22 Å). The initial fraction of mixing values for the 100-nm samples, $F_m(0)$, average 0.26. The magnitude of $F_m(0)$ has been attributed to the extent of deformation, and hence the void size, between particles.[22]

At 42 °C, there is virtually no further intermixing after the initial film formation. At 60 °C we calculate an increase of about 10% mixing over the initial value. It is only at 80 and 100 °C that the samples are predominantly intermixed; i.e., over 75% of the volume can be described as interdiffused. As a measure of the maximum amount of mixing obtainable, the colabeled control film yields an F_m of 0.95. It is interesting that it requires considerable thermal energy to impart thorough mixing, in light of the fact that many latex applications do not involve curing at temperatures significantly above the T_g.

B. Results Correlated with Transmission Electron Microscopy. Micrographs of a BMA film cured at 100 °C were obtained to ascertain whether the relative degree of interdiffusion between latex particles is visible over the same curing time scale as that detected by the fluorescence experiments. Figure 6 shows a micrograph of a BMA film (300-nm particle size) after the initial cure. This cross section of an 80% untagged BMA/20% AnMA-tagged BMA film is stained with RuO_4 to provide contrast to the anthryl-labeled phase. Since only image contrast, not energy transfer, is relevant, only anthryl-labeled BMA (which is selectively stained) is used. In cross section, the dodecahedral particles can appear as hexagons in a two-dimensional projection. Thus, the anthryl-labeled particles appear as the darker hexagonal shapes. The low level of phenyl ring-containing surfactant also stains enough to delineate particle boundaries of both labeled and unlabeled BMA.

Figure 7a shows a film cast from the same emulsion but cured at 100 °C for 10 min. We calculate a fraction of mixing of 0.45 at this stage. Note that the particle–particle boundaries have already started to blur, indicating some interdiffusion. However, at 10 min (Figure 7a) and even after 40 min of cure time (Figure 7b) it is possible to make out residual hexagonal structure. At later cure times of 5 and 48 h (Figure 8a,b), there are no observable particle

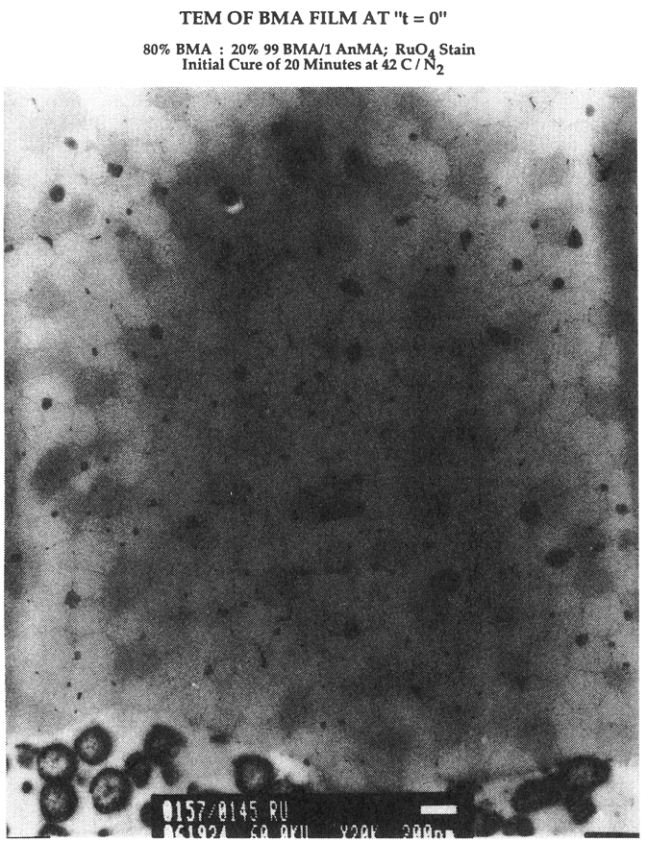

Figure 6. TEM micrograph of a BMA latex film after the initial precure. The anthryl-labeled particles are stained with RuO_4 and blended 20/80 with unstained particles. The interparticle boundaries are clearly visible.

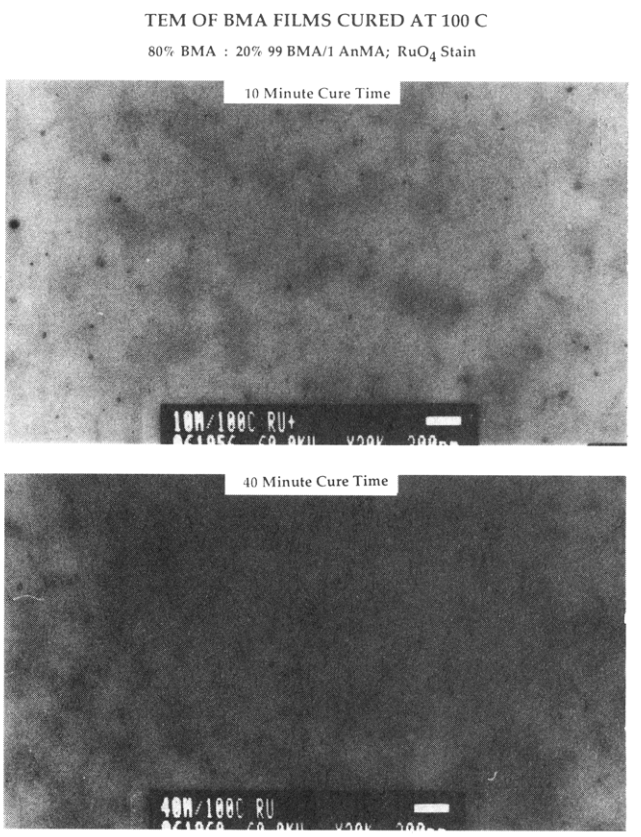

Figure 7. (a, Top) TEM micrograph of a BMA film. After curing for 10 min, the interparticle boundaries have started to blur, indicating that interdiffusion has begun. However, after 40 min (b, bottom), it is still possible to identify particle boundaries.

boundaries. Some very diffuse dark spots remain which could be assigned to the core of anthryl-labeled particles not yet invaded by unlabeled polymer. This may represent a highly entangled intraparticle region. In any case, the films appear to be significantly more interpenetrated than at the outset of the cure, and we measure a fraction of mixing of about 0.82 after 48 h.

C. Data Fit to the Spherical Diffusion Model. The data points in Figure 5 are fit to the spherical diffusion model at each temperature. We fit the F_m data to a power series in $t^{1/2}$ yielding coefficients a_0, a_1, a_2, and a_3. The reported D value is taken from the a_1 coefficient since this term is most important within the time scale of our experiments and has the lowest associated error. Table III lists the computed average D values for each sample tested.

There is some indication that we may be able to detect a shift in the time dependence of the mixing rate. According to Wool,[20] the number of monomer units crossing an interface scales with $t^{3/4}$ at times less than the reptation time when entangled chains are considered (as is the case here). The interdiffusion *length* scales with $t^{1/4}$ at $t < T_r$. It is reasonable to suspect that the initial relaxation of polymer chains on the particle surface would not follow simple Fickian diffusion and that the apparent increase in diffusant concentration at early time is from chain segments that relax across particle boundaries, without true center of mass diffusion of the polymer chain. This phenomenon has been alluded to recently by Pekcan,[24] who has noted a better fit of diffusion data to $t^{3/4}$ at earlier times.

The experimental observation that our data fit a Fickian model reasonably well cannot prove that the molecular motion involved satisfies Fick's law, since the system is subject to reptation. To understand the extent of interdiffusion in terms of de Gennes-type reptation concepts, the diffusion distance or the concentration profile, $C(r,t)$, must be obtained before invoking a Fickian diffusion model. Our recent efforts have focused on data for AmMA polymer cured at 60 °C. We are able to extract the diffusion length (distance), l, from our fraction of mixing data via rearrangement of eq 7. When the time dependence of the diffusion distance is allowed to vary, the best fit is obtained for t to the 0.42 power. This is an intermediate value between 0.25, predicted from a reptation model, and 0.5 for classic Fickian diffusion. Alternatively, different portions of the curve ($t <$ or $> T_r$) may be fit independently. A transition in the time dependence of our data appears to occur at a cure time on the order of the chain reptation time, but further data are needed to clarify the exact nature of the time dependence. This will be the focus of a subsequent paper.

It is also possible to calculate a cumulative diffusion coefficient that represents the diffusion rate constant at a certain point in time (or in our model, at a certain F_m). A cumulative D is computed by solving eq 8 at each experimental point. The cumulative D values decrease with time by at least an order of magnitude throughout. The variation in D with time is probably, in part, a reflection of the molecular weight dependence on diffusion. The lower molecular weight component of the sample would be expected to dominate the process at early time, while slower, higher molecular weight chains would contribute more at later time.

Another feature of these data is the change in curvature of the fits at longer times. In the data for the 80 °C cure (Figure 5), there is a local minimum in the curve at about 41 $min^{1/2}$. At this point the fit to the spherical diffusion

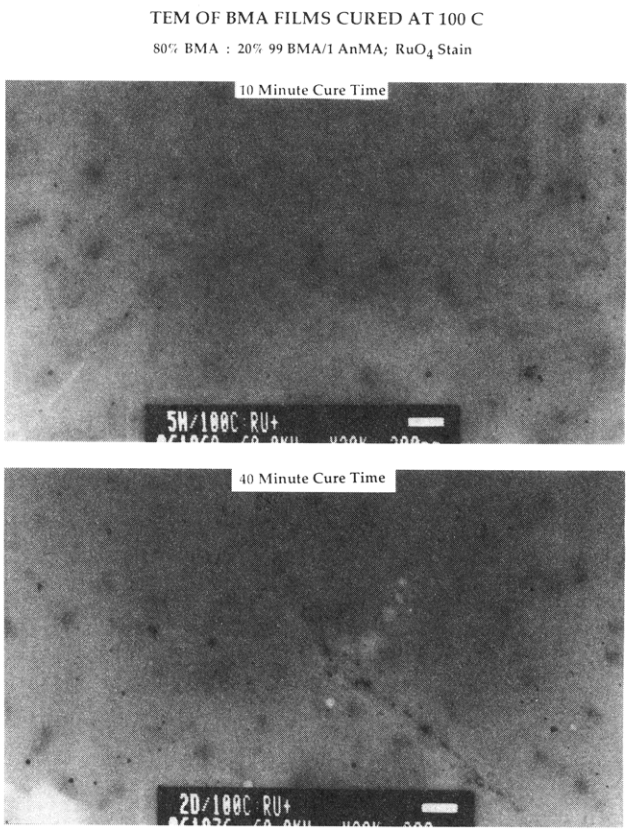

Figure 8. (a, Top) TEM micrograph of a BMA film. After curing for 5 h, the particle boundaries have disappeared completely. The stained areas remaining are the residual unmixed portions of the films. (b, Bottom) Curing for 48 h corresponds to a fraction of mixing of 0.82, near the maximum observable mixing for this system.

Table III. Average Polymer Self-Diffusion Coefficients ($\times 10^{-16}$ cm^2/s)

sample	42 °C	50 °C	60 °C	70 °C	80 °C	100 °C
BMA (100 nm)	0.00035		0.028		0.23	5.4
BMA (300 nm)					0.76	4.0
AmMA (100 nm)	0.0044	0.023	0.53	1.0	5.7	
			0.32	1.3	2.2	

model begins to break down and the calculated curve begins to increase rapidly. The diffusion length, l, at 50 min$^{1/2}$ is equal to 45 nm. This distance is converging on the boundary conditions of our model, i.e., the particle radius of 53 nm.

We may compare the diffusion coefficients calculated in our experiment with those of ref 18 and with values arrived at by entirely different techniques. Winnik has also used the nonradiative energy transfer technique, but with a different donor/acceptor pair. Hahn and coworkers[4] determined diffusion coefficients using small-angle neutron scattering techniques on BMA polymers of two different molecular weights. Whitlow and Wool,[20] using SIMS to measure depth profiles in partially deuterated polystyrene as a function of temperature and molecular weight, also calculated diffusion coefficients. Values for comparison are listed in Table IV. We see that even with differing experimental details (temperature, molecular weight, etc.), the diffusion coefficients agree to better than an order of magnitude for the same polymer.

D. Data Fit to the Arrhenius Equation. For the BMA composition at different temperatures (Figure 5) we observe that the average diffusion coefficient changes 4 orders of magnitude on going from 42 °C ($D = 3.5 \times 10^{-20}$ cm^2/s) to 100 °C ($D = 5.4 \times 10^{-16}$ cm^2/s). In the case of

Table IV. Comparison of Diffusion Coefficients from Various Sources

polymer	particle size (nm)	M_w[a] (×1000)	cure temp/ time (min)	ref	D ($\times 10^{-16}$ cm^2/s)
BMA	100	384/372	80/avg $T - T_g = 47$	this work	0.23
BMA	100	384/372	100/avg $T - T_g = 67$	this work	5.4
BMA	300	333/311	100/avg $T - T_g = 67$	this work	4.02
BMA	135/116	630/550	90/10 90/2316 $T - T_g = 60$	18	3.41 0.99
BMA	30	500	90/30 90/600 $T - T_g = \sim 60$	4	4.7 ● 2.0 2.2 ● 0.6
PS	soln	169/199	125/362 147/30 $T - T_g = 19, 41$	20	1.403 86

[a] Two values denote different labels.

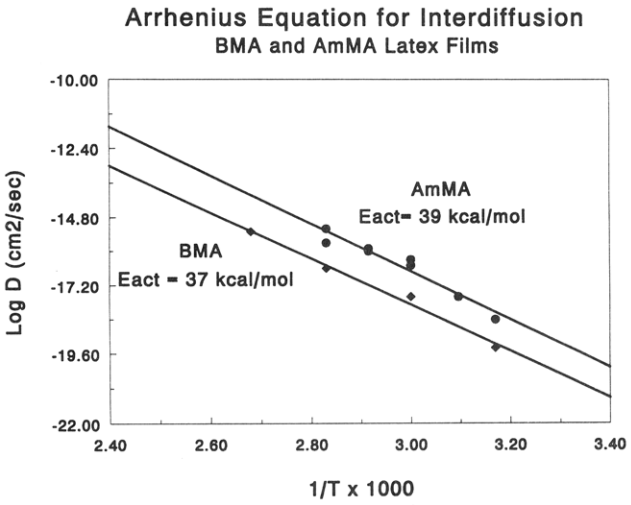

Figure 9. Arrhenius plot showing the temperature dependence of the diffusion coefficients for AmMA and BMA polymers, calculated from the spherical diffusion model. The activation energies are calculated directly from the slopes of the lines.

BMA, heating to at least 30 °C above the glass transition temperature is required to create even a semimixed system on the order of hours. An Arrhenius plot of log D versus $1/T$ is found in Figure 9, which demonstrates an excellent linear correlation, although over a relatively narrow temperature range. We compute an apparent activation energy of 37 kcal/mol for interdiffusion in BMA. This energy barrier corresponds to the amount of thermal energy required to initiate interdiffusion by overcoming cohesive forces and creating free volume. We also note that Winnik[10] arrives at a value (38 kcal/mol) nearly identical to that produced in this work. Furthermore, a value of 37 kcal/mol was reported by Ferry in 1958,[25] measured using a dynamic mechanical technique to probe the α transition in BMA. Thus, the apparent activation energy we measure for diffusion throughout this temperature range is comparable to the activation energy for the local segment rearrangement in the polymer that commences at T_g.

E. Effect of Particle Size. Two nearly identical sets of labeled BMA latices were prepared with particle sizes of 100 and 300 nm (see data in Table II). Figure 10 shows the fraction of mixing versus time curves for films of both particle sizes when cured at 100 °C for up to about 100 min. As shown, the mixing rate is more rapid in the smaller particle size latex. This is what is expected intuitively, based on consideration of the surface area to volume ratios.

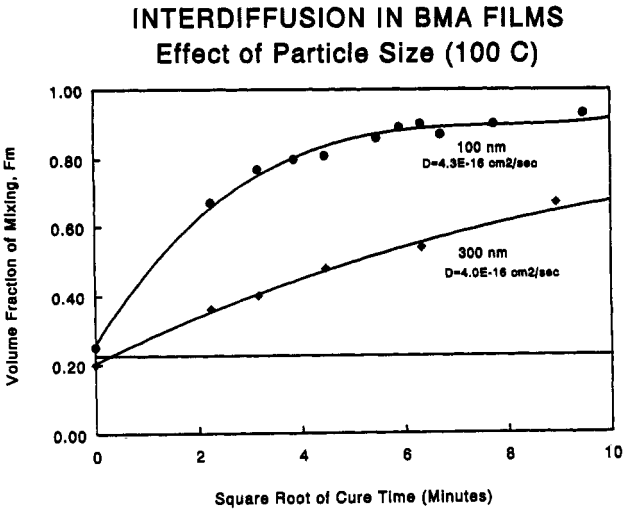

Figure 10. Plots of F_m versus cure time for BMA latices of two different particle sizes. Although the diffusion coefficients are similar, interparticle mixing is faster in the 100-nm latex, in accord with predictions from the model.

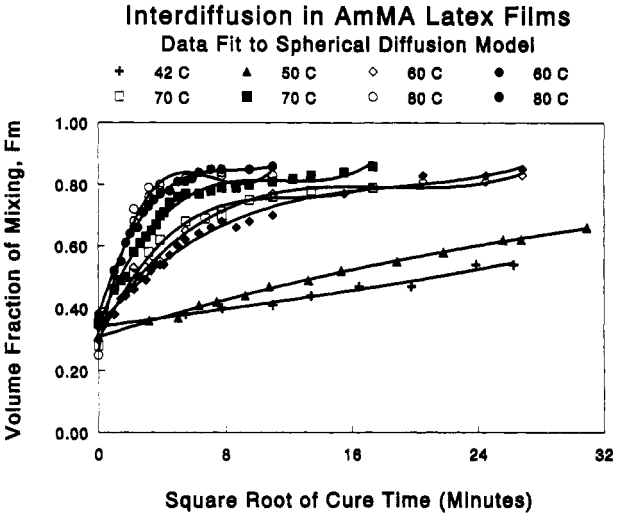

Figure 11. F_m versus cure time for AmMA films. Note the more rapid film interdiffusion when compared to BMA (Figure 4) for this lower T_g polymer. Controls are also indicated on the figure by single points.

The dependence of the interparticle mixing rate on the particle size is $1/R$, both according to eq 9 and according to a surface area/volume ratio. We calculate roughly equivalent D values for these two samples. The diffusion coefficients should be similar since the polymer compositions are identical and very similar in molecular weight. However, the mixing rate is about 3 times greater for the 100-nm particles. Rudin[26] has demonstrated the decrease in the degree of interparticle fusion (and also slight increase in MFFT) with increasing particle size in MMA/BA/AA films using scanning electron microscopy.

F. Effect of Polymer Composition. A series of amyl methacrylate (AmMA) copolymers was also prepared to study interdiffusion in a polymer with a lower T_g and also to test the influence of the compatibility of polymer blends on the extent of mixing. The curves of fraction of mixing versus cure time for the AmMA homopolymer at different cure temperatures are shown in Figure 11. Repeat runs at 60, 70, and 80 °C are included, and the diffusion coefficients are listed in Table III. The effect of the lower T_g (17 °C) when compared to the BMA homopolymer is evident in the higher rate of interdiffusion at comparable temperatures. For example, at both 60 and 80 °C, the diffusion rate in the AmMA polymer is over an order of

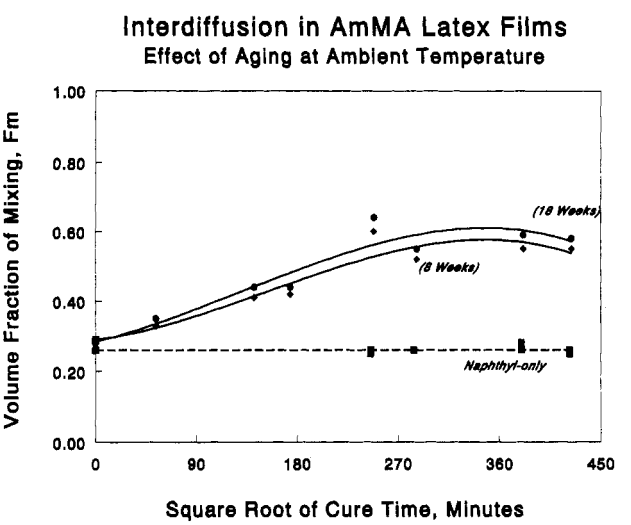

Figure 12. AmMA films cured at ambient temperature for long times indicate that slow mixing can occur in a polymer with a T_g near room temperature. The control film remains stable.

magnitude faster than in BMA. The original data at 42 °C show an induction time before diffusion commences. We attribute this occurrence to insufficient drying and coalescence at this temperature. Since the initial cure time was somewhat arbitrary and was purposely kept to a minimum to avoid overcuring, we adjust time zero to the point where mixing actually starts. In fact, if t_0 is allowed to vary in the calculation of the diffusion coefficient, the best fit comes when t_0 is equal to about 30 min at 42 °C and 5 min at 50 °C.

It is also interesting that with the AmMA films, in contrast to the BMA, it is possible to detect some mixing under ambient conditions, albeit at very long times. Figure 12 depicts F_m versus time curves over an 18-week duration at room temperature. The level of interpenetration slowly rises to about 0.55. Polymers similar in hardness to AmMA might typically be applied at room temperature, and thus interdiffusion can be expected to occur as the system slowly cures on a time scale of months. This observation could have relevance when considering how long a film must be cured to develop certain performance properties.

The Arrhenius plot for AmMA is also found in Figure 9. We calculate an apparent activation energy of 39 kcal/mol for AmMA. This value is nearly identical to that for BMA (37 kcal/mol), and the difference is probably within our overall experimental error. Interpolating from the results of dynamic mechanical experiments by Ferry,[25] the E_{act} for viscoelastic relaxation in AmMA should be roughly 32 kcal/mol for α motions. Ferry observed a trend of decreasing E_{act} with increasing side chain length in a series of methacrylate films. As Ferry's work yielded an activation energy strictly from analysis of the temperature dependence of the mechanical response at T_g, our results may point to the added influence of other types of cooperative motion required for center of mass diffusion, particularly the added friction from the longer side chain. Another factor to consider is whether the details of the polymer structure are significantly different. The AmMA polymer may possess more branching or a different molecular weight distribution than the BMA composition.

The temperature dependence of diffusion may also be expressed through the WLF equation, derived from the dependence of viscosity on the fractional free volume, which increases linearly with temperature above T_g. A WLF temperature dependence is observed for many polymer properties, including diffusion. According to WLF theory, the apparent activation energy should be

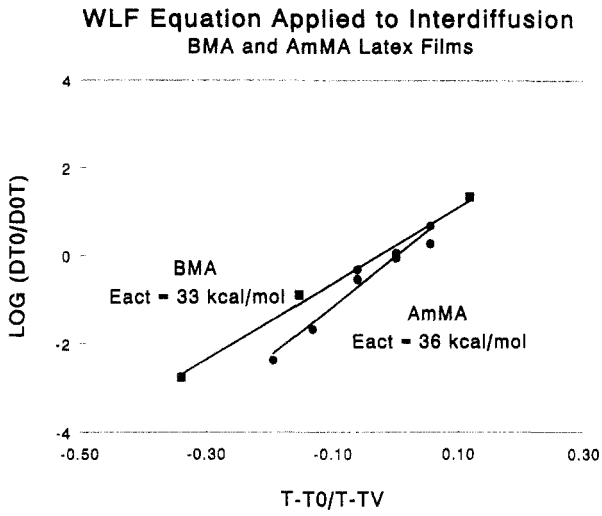

Figure 13. Temperature dependence of the AmMA and BMA diffusion coefficients plotted according to the WLF equation. The reference temperature was chosen as 80 °C for BMA and 70 °C for AmMA, 47 and 52 °C above T_g, respectively. The data yield essentially equivalent activation energies.

independent of structure (except as structure is manifested in the T_g itself) and depend only on the T_g. Figure 13 depicts a plot of the WLF equation in the form of

$$\log(DT_0/D_0T) = C_1(T - T_0)/(T - T_\infty) \qquad (12)$$

at the reference temperature T_0 (approximately 50 °C above T_g), where T_∞ is the so-called Vogel temperature, D_0 is the diffusion coefficient at T_0, and C_1 is a constant defined at T_0. For BMA, it has been found that the valid range for application of the WLF equation to viscoelastic data is 45–135 °C.[27] Calculating activation energies using a WLF approach via the relation[27]

$$\Delta H = 2.303RT^2C_1C_2/(C_2 + T - T_0)^2 \qquad (13)$$

where $C_2 = T_0 - T_\infty$, yields 33 and 36 kcal/mol, respectively, for BMA and AmMA. Again, the activation energies for AmMA and BMA are almost identical. In a free volume theory description of the WLF constants, C_1 (the slope in Figure 13) is related to the minimum hole size for polymer segment displacement. The close agreement for activation energies obtained via an Arrhenius or WLF approach is probably a consequence of the relatively narrow temperature range explored.

Additional experiments were also undertaken to probe the influence of polymer compatibility on interdiffusion in blends of two polymer compositions. For this purpose, films cast from a 50/50 blend of either anthryl-tagged BMA with naphthyl-tagged AmMA or naphthyl-tagged BMA with anthryl-tagged AmMA were used. When dealing with polymer particles tagged with one member of a donor/acceptor pair, studying a blend introduces added heterogeneity into the system, in that the naphthyl group may be located on either the AmMA or BMA chains. Strictly, the Förster equation should be rewritten to include terms representing the three possible domains that now exist, rather than two (AmMA-rich, BMA-rich, and unmixed). Duplicating the fluorescence experiment with the donor/acceptor moieties tagged alternately on one or the other of the components indicates that in the BMA/AmMA blend there are some differences in the F_m vs time curves, depending on the location of the tag molecules. This is probably a result of differences in the details of the labeling in one polymer system versus another. Nevertheless, we fit the data in the standard fashion, recognizing the limitations of any quantitative analysis.

Interdiffusion in Polymer Blends

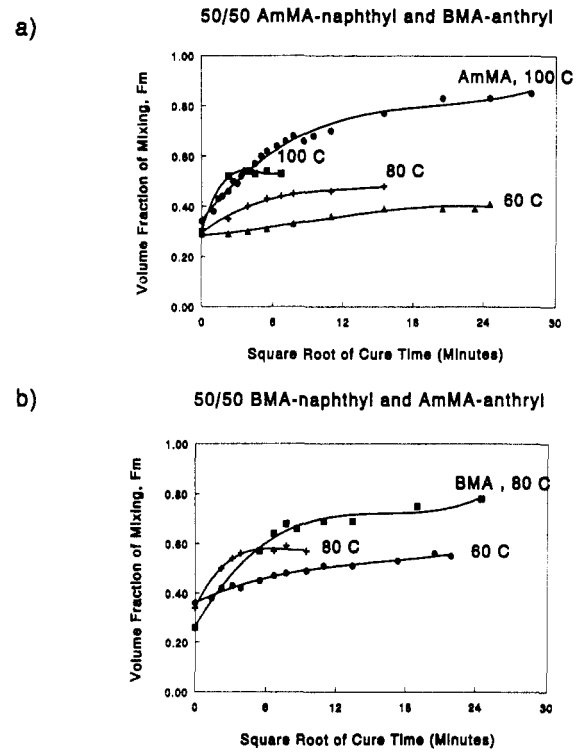

Figure 14. (a) F_m versus cure time curves for a polymer blend of AmMA and BMA latices where the AmMA portion is tagged with naphthyl chromophore and the BMA portion is tagged with anthryl. (b) Analogous plots for films in which the naphthyl group is bound to the BMA and the anthryl is bound to the AmMA. Data from the homopolymer films are also provided for comparison. The lack of total miscibility between the blend components limits interdiffusion.

Figure 14 portrays the outcome of these experiments on blends of AmMa and BMA when the naphthyl tag is incorporated into either the AmMA component (Figure 14a) or the BMA component (Figure 14b). In both cases, comparisons are best made with the earlier data for the corresponding homopolymer. In general, we observe that the blends have a significantly lower extent of mixing than the homopolymer controls (naphthyl-tagged AmMA/anthryl-tagged AmMA for Figure 14a, or naphthyl-tagged BMA/anthryl-tagged BMA for Figure 14b). The lack of total miscibility between the two compositions appears to limit the interdiffusion. The mixing rate in the blends does increase with increasing temperature, but the final F_m achieved is much less than in either pure component. Since compatibility increases with decreasing molecular weight, the mixed fraction may represent interdiffusion of the lower molecular weight species that are able to mix on a molecular level.

It is possible to calculate the solubility parameters (δ), after the manner of Krauss[28] for the species involved in the blend. Using molar attraction constants tabulated by Small,[29] we estimate the interaction parameter, χ, for the blend pair at room temperature, using

$$\chi \approx (\delta_A - \delta_B)^2/6 = 0.0017 \qquad (14)$$

A general rule is that a χ value less than or equal to 0.002 is required for miscibility at this molecular weight;[30] thus this composition is borderline for miscibility. Blends of AmMA with poly(styrene-*co*-butyl acrylate) and AmMA with poly(butyl acrylate-*co*-methyl methacrylate) were also investigated. These blends show almost no decrease in naphthyl lifetime, indicating virtually no interdiffusion

when cured for 4 h at 80 °C. This observation agrees with the trend of higher interaction parameters calculated for these systems.

DSC scans of the blends have failed to give indication of more than one glass transition temperature, usually taken as evidence of the presence of multiple phases. However, the T_g's of the blend components are fairly close, making resolution a problem and demonstrating the greater capability of the fluorescence technique to distinguish multiple phases.

V. Conclusion

The application of NET to nascent latex films adds valuable insight into the details of the diffusion process and the effects of simple compositional and structural variables. Clearly, the rate and extent of polymer interdiffusion are sensitive functions of many of the variables encountered in emulsion technology. This work describes recent studies of a few of the parameters most relevant to the coatings industry. The effect of particle size can be quantitatively accounted for by a simple geometric description of diffusion. Compositional changes in the latex accelerate interdiffusion when the polymer T_g is lowered and inhibit interdiffusion when the latex blend is comprised of incompatible polymers. In addition, we verify the conceptual picture afforded by the fluorescence measurements with images obtained via transmission electron microscopy.

Use of the naphthyl/anthryl energy transfer pair achieves results that are analogous to those obtained through use of the phenanthryl/anthryl pair employed by Winnik. The differences in chemical details between the two donor chromophores will provide another choice of labels for further studies. Our observation that a simple geometric model can yield an adequate description of the time dependence of interdiffusion suggests that additional details of the diffusion process may be hidden in he fluorescence decay curves. To choose the correct mathematical formalism, however, we will continue to work to extract more accurate parameters from the analysis of the lifetime data.

Acknowledgment. The authors would like to thank Dr. John Reffner, Dr. Robert Antrim, Ms. Charlene Trader, and Ms. Dorrie Holden for the microscopy work, Mr. John Simmons for the DSC data, Ms. Donna Grecian and Dr. Walt Platek for the GPC results, and Dr. Pete Sperry and other members of the Film Formation Forum at Rohm and Haas for helpful discussions and ideas. We would also like to acknowledge the Rohm and Haas Co. for support of this work.

References and Notes

(1) Brown, G. L. *J. Polym. Sci.* **1956**, *22*, 423.
(2) Vanderhoff, J. W. *Br. Polym. J.* **1970**, *2*, 161.
(3) Voyutskii, S. S.; Ustinova, Z. M. *J. Adhes.* **1977**, *9*, 39.
(4) Hahn, K.; Ley, G.; Schuller, H.; Oberthur, R. *Colloid Polym. Sci.* **1986**, *264*, 1092.
(5) Hahn, K.; Ley, G.; Oberthur, R. *Colloid Polym. Sci.* **1988**, *266*, 631.
(6) Linne, M. A.; Klein, A.; Miller, G. A.; Sperling, L. H. *J. Macromol. Sci., Phys.* **1988**, *B27*, 217.
(7) Yoo, J. N.; Sperling, L. H.; Glinka, C. J.; Klein, A. *Macromolecules* **1990**, *23*, 3962.
(8) Yoo, J. N.; Sperling, L. H.; Glinka, C. J.; Klein, A. *Macromolecules* **1991**, *24*, 2868.
(9) Pekcan, O.; Winnik, M. A.; Croucher, M. D. *Macromolecules* **1990**, *23*, 2673.
(10) Zhao, C.-L.; Wang, Y.; Hruska, Z.; Winnik, M. A. *Macromolecules* **1990**, *23*, 4082.
(11) Fox, R. B.; Cozzens, R. F. *Macromolecules* **1969**, *2*, 181.
(12) Shiah, T. Y.-J.; Morawetz, H. *Macromolecules* **1984**, *17*, 792.
(13) (a) Förster, T. *Ann. Phys.* **1948**, *2*, 55. (b) Förster, T. *Discuss. Faraday Soc.* **1959**, *27*, 7.
(14) Berlman, I. B. *Energy Transfer Parameters of Aromatic Compounds*; Academic Press: New York, 1973; p 309.
(15) Bennett, R. G. *J. Chem. Phys.* **1964**, *41*, 3037.
(16) Pekcan, O.; Egan, L. S.; Winnik, M. A.; Croucher, M. D. *Macromolecules* **1990**, *23*, 2210.
(17) (a) Birks, J. B. *Photophysis of Aromatic Molecules*; Wiley-Interscience: New York, 1970; p 571. (b) *Ibid.*, pp 569. (c) *Ibid.*, p 126.
(18) Wang, Y.; Zhao, C.-L.; Winnik, M. A. *J. Chem. Phys.* **1991**, *95*, 2143.
(19) Crank, J.; Park, G. S., Eds. *Diffusion in Polymers*; Academic Press: New York, 1968.
(20) Whitlow, S. J.; Wool, R. P. *Macromolecules* **1991**, *24*, 5926.
(21) Pekcan, O.; Winnik, M. A.; Croucher, M. D. *J. Polym. Sci., Polym. Lett. Ed.* **1983**, *21*, 1011.
(22) Winnik, M. A.; Wang, Y.; Haley, F. *J. Coat. Technol.* **1992**, *64*, 51.
(23) Trent, J. S.; Scheinbeim, J. I.; Couchman, P. R. *Macromolecules* **1983**, *16*, 589.
(24) Pekcan, O.; Canpolat, M.; Göçmen, A. *Eur. Polym. J.* **1993**, *29*, 115.
(25) Ferry, J. D.; Strella, S. J. *J. Colloid Sci.* **1958**, *13*, 459.
(26) Eckersley, S. T.; Rudin, A. *J. Coat. Technol.* **1990**, *62*, 89.
(27) (a) Ferry, J. D. *Viscoelastic Properties of Polymers*, 3rd ed.; John Wiley & Sons, Inc.: New York, 1980; p 310. (b) *Ibid.*, p 289.
(28) Krauss, S. In *Polymer Blends*; Paul D. R., Newman, S., Eds.; Academic Press: New York, 1978; pp 15–113.
(29) Small, P. A. *J. Appl. Chem.* **1953**, *3*, 71.
(30) David, D. J.; Sincock, T. F. *Polymer* **1992**, *33*, 4505.